

MEASUREMENTS OF THE FIRST RF PROTOTYPE OF THE SPIRAL2 SINGLE BUNCH SELECTOR*

M. Di Giacomo[#], GANIL/Spiral2, Caen, France

A. Caruso, G. Gallo, E. Zappalà, D. Rifuggiato, A. Longhitano, INFN-LNS, Catania, Italy
 F. Consoli, Associazione Euratom-ENEA sulla Fusione, CP 65-00044 Frascati, Rome, Italy

Abstract

The single bunch selector of the Spiral2 driver uses 100 Ω travelling wave electrodes driven by fast pulse generators. 2.5 kV, 1 kW feedthroughs and a vacuum chamber housing the water cooled electrodes have been designed and built. The paper reviews the whole design and reports the results of first RF and power measurements.

INTRODUCTION

The single-bunch selector (SBS) of the Spiral2 accelerator reduces the bunch repetition rate onto the experimental target of a factor 100 to 10000. To reduce the power required to perform this operation, the device uses a static magnetic field deflecting the beam towards a beam dump, and two short pulses of opposite sign travelling along high impedance (100 Ω) meander ($\beta=v/c=0.04$) electrodes, selecting the bunch to be deflected. The RF part of the device is still in a detailed design phase and a prototype of vacuum chamber, equipped with water cooled electrode housings, and high power 100 Ω couplers (or feedthroughs: FT) has been recently designed, built and measured. The paper reports the mechanical design concept and relates the results of power, high voltage and RF measurements.

MECHANICAL DESIGN

The vacuum chamber design (Fig. 1) aims to minimize the gap of the outer magnet, to simplify the electrode and FTs assembling and the cooling circuit brazing.

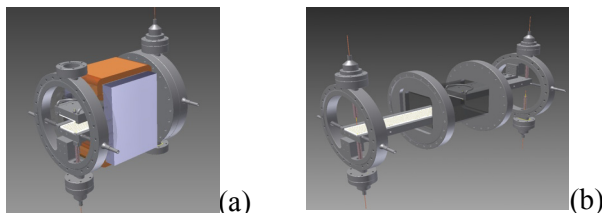


Figure 1: a) Sketch of the complete device (magnet and travelling-wave electrodes); b) assembly principle.

Each electrode housing is then supported by its own ring flange, which hosts the water outlets and one of the two feedthroughs for the electrode. The housing is made of copper (Fig.2), because it constitutes the ground plane of the meander line and is water cooled to dissipate the RF power (mainly located in the meander strip) and the

particle beam losses. These last could be reduced by slits at the meander entrance, which do not exist on this prototype but could be added easy. The alumina plate is screwed to the housing to obtain proper RF characteristics, Z_c and delay, as shown in Fig. 2b. Under vacuum, there is no significant heat transfer through the bottom ceramic surface, thus the housing is designed in such a way that its side elements are pushed against the ceramic plate sides, to grant lateral thermal conduction. A thin layer of Indium is inserted to improve the contact surface. After assembling each electrode, the two parts are inserted from opposite sides into the closing cylindrical chamber. The second FT of each electrode is finally inserted and connected. To braze the inner wire to the meander strip, the ceramic plate is warmed up with a hot air gun (400°C).

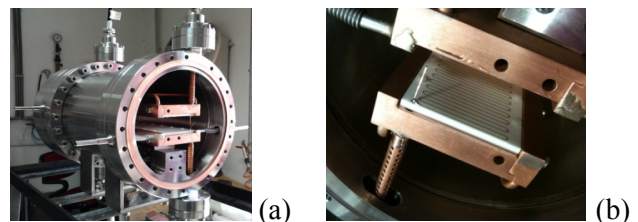


Figure 2: a) SBS prototype and b) details of the electrode and feedthrough assemblies.

DC POWER MEASUREMENTS

Each electrode has been driven with a 60V, 10A, DC power supply, to measure the static strip resistance, the plate temperature profile, the assembly out-gazing and to search for the current limits of the meander.

Strip Resistance

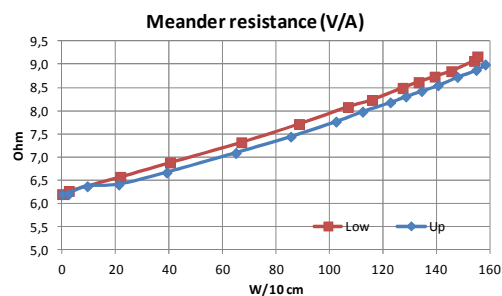


Figure 3: Strip resistance vs loss density, for the upper and lower electrode.

The meander resistance changes with the temperature of the plate. It can be measured from the voltage to current V/I ratio as shown in Fig 3. The power lost is

*Work supported by EU commission 7th framework project n. 212692.
[#]digiacom@ganil.fr

given by the product $V \cdot I$. The plate is 273 mm long and loss is expressed for an equivalent 10 cm long structure, in order to facilitate comparisons between structures of different length.

Plate Temperature Profile

Fig. 4a shows the simulated temperature map with loss of 273 W (100W/10cm). Temperature is maximum along the longitudinal axis and side cooling effect is clearly visible.

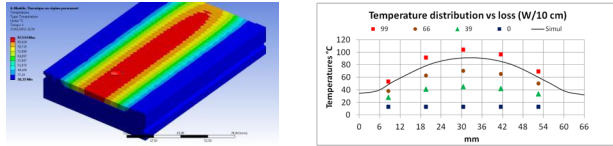


Figure 4: Temperature profiles.

Figure 4b shows temperature values at different loss level, measured along a section far from the extremity. Maximum values are slightly higher than expected and rise over 100°C.

Outgassing

Vacuum measurements have shown that convection disappears for chamber pressure $< 10^{-1}$ mbar and that total outgassing of the structure is around $1 \cdot 10^{-7}$ Pa·m²·s⁻¹, after the baking treatment due to the DC power measurements. This is more than three times better than expected at 20°C and the margin compensates the additional outgassing due to operating temperature up to 100°C.

Meander Current Limits

Power tests on the first prototype of the meander plate had shown [1] that the rectangular shape of the strip u-bend could burn around 90 W/10cm. Several weak u-bends had burnt out (and repaired) before the strip could be burnt on a point located along the longitudinal axis (the hottest area). The new strip (Fig. 5), thought slightly narrower, could stand more than 160 W/10 cm. We couldn't go higher, having reached the maximum value of the power supply voltage (60 V, 10 A).

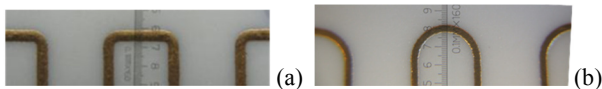


Figure 5 : old (a) and new (b) u-bend design.

More details concerning all these measurements are reported in [2].

HV MEASUREMENTS

The system is designed to receive fast and short high voltage pulses up to 2.5 kV. Break-down limits have been tested with a DC generator up to 3.3 kV, when a first spark appeared at one of the input N connectors. No sparks were observed on the elements under vacuum.

RF MEASUREMENTS AND ANALYSIS

We perform all measurements with a vector analyzer, using 50 Ω normalized impedance and matching loads.

A bandwidth (300 MHz) twice larger than the spectrum covered by the pulse signal [3] is chosen.

Our ultimate goal is to know how the pulses are transformed along the meanders. Therefore, we need to characterize with transmission matrix ABCD all the components of the RF chain (cables, feedthroughs, meanders, matching load) over a large enough frequency band. The complete set of scattering parameters (S_{11} , S_{21} , S_{12} , S_{22}) is thus measured in the 0.1÷300 MHz bandwidth, with the highest possible resolution (1600 points).

As connectors and unknown transitions are added to interface the single element to the network analyzer ports, an analytical deembedding is required to extract the scattering parameters of each element from the rough measurements. The method is described in [3] and has already been implemented for the single meander and for the single FT. The analysis of a meander assembled with input and output FTs still has to be performed. S parameters measured on 50 Ω can also be transformed into 100 Ω with the formula

$$\bar{S}_{100} = \left\{ 50 [\bar{I} + \bar{S}_{50}] \cdot [\bar{I} - \bar{S}_{50}]^{-1} - 100 \bar{I} \right\} \cdot \left\{ 50 [\bar{I} + \bar{S}_{50}] \cdot [\bar{I} - \bar{S}_{50}]^{-1} + 100 \bar{I} \right\}^{-1} \quad (1)$$

to have a clearer view of the amount of matching.

Feedthrough Results

The four single FTs [4] have been measured and Fig. 6 shows one of them equipped with input and output connectors and the modulus of the S_{11} parameter.

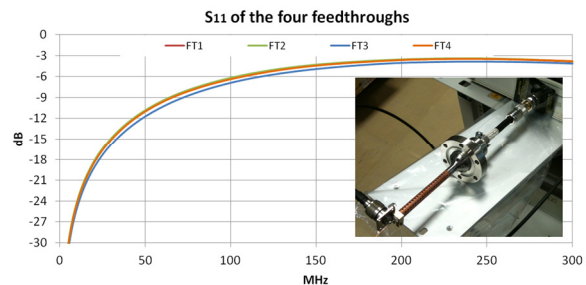


Figure 6 : Measured S_{11} parameter, with 50 Ω reference, of the four FTs equipped with 100Ω cable and input and output standard N connectors.

FT #3 is slightly different from the three others. Anyway, the four of them behave a little differently than expected. This is mainly due to the deformations present on the inner conductor of the vacuum side coaxial line. The 1 mm section wire is both undulated and not perfectly coaxial, and the resulting characteristic impedance of this section is around 85 Ω, as shown in Fig. 7. The S_{12} parameter is chosen as the dependence on the coaxial Z_c is more visible than on the other S parameters.

Simulations performed on the coaxial line alone have also shown that the contribution of the average position offset of the inner conductor, dominates the impedance reduction, while the number of (half) oscillation is less important.

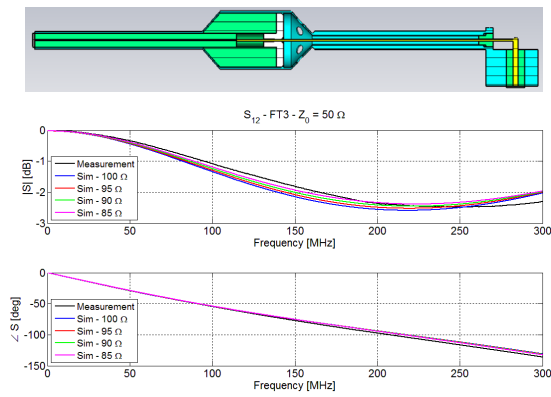


Figure 7: CST Microwave Studio simulation geometry and results of measurements fitting.

In Fig 8, the inner conductor is first positioned straight and on axis or off-axis, giving the lowest (red) and highest (green) curves of the plot. Then, sinusoidal undulations of the same amplitude of the offset are considered. In this case the structure is slightly mismatched, but less than in the green case and no significant differences can be appreciated increasing the half-oscillation number.

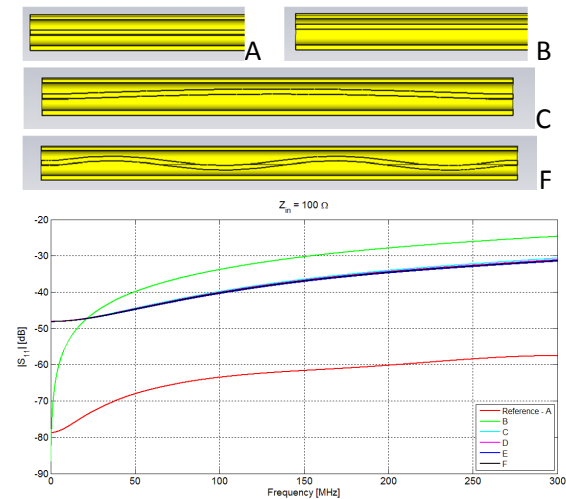


Figure 8: Effect of offset and undulations for the different structures. C, D, E, F have 0.5, 1, 1.5 and 2 - oscillations, respectively, as shown just for C and F.

Meander Results

The two assembled meanders (meander+FT) appear to be perfectly symmetrical ($S_{11} = S_{22}$ and $S_{12} = S_{21}$), confirming that the small difference observed on FT3 with respect to the others is negligible. Nevertheless, both S_{11} and S_{21} patterns shown in Fig. 9 are different. A preliminary, simple analysis based on an analytical fitting performed with a model of cascaded transmission line sections, leads to the following results: the two meanders (plate + housing) have different impedance Z_c and delay. Z_c values of 106 Ω (down) and 109 Ω (up) are estimated from the pattern maxima, while the β of the two structures are respectively of 0.04 and 0.042 (estimated from the FT delays and the pattern periodicity).

CONCLUSION

Most of design goals: vacuum, power cooling and high voltage issues have been achieved. The system has been safely operated at 100W/10cm, DC, and withstands higher voltages (> 3.3 kV, DC) than required (< 2.5 kV, 19 ns pulse).

Differences between the delays (5%) and impedances (3%) of the two electrodes have been observed. The problem origin has been identified and the Up housing is being modified to achieve a smoother and more planar surface in order to improve RF parameter matching.

Numerical de-embedding analysis is being continued to obtain independent S parameters of all components.

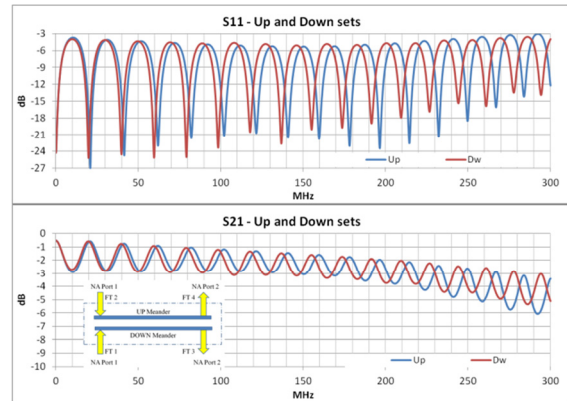


Figure 9 : S_{11} and S_{21} parameters of the Up and Down sets of meander+2FT assembled inside the vacuum chamber.

ACKNOWLEDGMENT

The authors are grateful to P. Balleyguier for his suggestions, to P. Sarta and G. Manno for their help solving the problems encountered during the preparation of the test bench, to P. Toussaint who proposed the conceptual design of the present assembly principle, to C. Barthe-Dejean, and Ph. Robillard for thermal and vacuum modeling.

REFERENCES

- [1] P. Balleyguier, et al., "Electrode Design Improvements in the SPIRAL2 Single Bunch Selector", LINAC2010, Tsukuba, September 2010, MOP098, p.286.
- [2] M. Di Giacomo et al., "Test Report of the Prototype of the SBS chamber with the Electrode Housings and Second Set of Meander Plates", Ganil-Spiral2, EDMS I-030233.
- [3] F. Consoli et al., "Broadband Characterization of the 100 Ω Electrode Features of the SPIRAL2 Single Bunch Selector by Scattering Parameter Measurements", submitted to Physical Review Special Topics - Accelerators and Beams.
- [4] F. Consoli et al., "RF Design of the Power Coupler for the SPIRAL2 Single Bunch Selector", PAC11, New York, May 2011, TUP277, p.1346.